www.elsevier.com/locate/ijmactool

Model Based Reconstruction of Milled Surface Topography from Measured Cutting Forces

B. Denkena, M. Krüger, D. Bachrathy, G. Stepan

PII: S0890-6955(11)00242-2
DOI: doi:10.1016/j.ijmachtools.2011.12.007
Reference: MTM 2721

To appear in: *International Journal of Machine Tools & Manufacture*

Received date: 3 August 2011
Revised date: 13 December 2011
Accepted date: 15 December 2011

Cite this article as: B. Denkena, M. Krüger, D. Bachrathy and G. Stepan, Model Based Reconstruction of Milled Surface Topography from Measured Cutting Forces, *International Journal of Machine Tools & Manufacture*, doi:10.1016/j.ijmachtools.2011.12.007

Model Based Reconstruction of Milled Surface Topography from Measured Cutting Forces

Authors: Denkena, B.*; Krüger, M.*; Bachrathy, D.**; Stepan, G.***

* Institute of Production Engineering and Machine Tools,
Leibniz Universität Hannover,
Garbsen D-30823, Germany
e-mail: krueger@ifw.uni-hannover.de

** Research Group on Dynamics of Vehicles and Machines,
Hungarian Academy of Sciences,
Budapest H-1111, Hungary
e-mail: bachrathy@mm.bme.hu

*** Department of Applied Mechanics,
Budapest University of Technology and Economics,
Budapest H-1111, Hungary
e-mail: stepan@mm.bme.hu

Abstract:
This paper presents a method for the reconstruction of surface topographies of peripheral milled surfaces based on measured cutting forces. Even under stable process conditions, machine tool vibrations occur due to the milling tool's dynamic excitation. In order to estimate the influence of tool vibrations on surface degradation, a dynamic tool model is developed and applied to a material removal model. The proposed tool model is able to reconstruct the accurate shape and roughness of machined surfaces. The developed method is verified by comparing the reconstructed and the measured surface topographies. The results demonstrate that the method is able to reconstruct the surface topography of the machined workpiece from measured resultant cutting forces and it can be used also for the online monitoring of milling processes.

Keywords:

Dynamic endmill model, force measurement, machine tool vibrations, quality monitoring, milling process

Nomenclature

a_e	Width of cut	[mm]
a_p	Depth of cut	[mm]
A	Cross-section of the endmill	[mm^2]
$\mathbf{b}$	Boundary curve of the cross-section	[mm]

B_l	Modal constant of the l^{th} natural frequency of the spindle	[1/kg]
f_{te}	Tooth engagement frequency	[Hz]
$\mathbf{f_z}$	Feed per tooth vector	[mm]
$\mathbf{F}$	Resultant force vector	[N]
I_{xx}, I_{yy}, I_{xy}	Moments of inertia	[mm^4]
i	Index of the cutting edge	[1]
j	Index of the incremental heigth	[1]
k	Index of polygon knots	[1]
$\mathbf{M}, \mathbf{C}, \mathbf{K}$	Mass, damping and stiffness matrices	[kg,kg m^2] [Ns/m,Nms/rad] [N/m,Nm/rad]
l	Number of polygon knots	[1]
n	Spindle speed	[min^{-1}]
N	Number of cutting edges	[1]
N_{act}	Number of the active segments of the endmill	[1]
N_m	Number of eigenmodes	[1]
$\mathbf{p}$	Tool path vector	[mm]
q_l^s	Modal coordinates of the spindle	
R	Radius of the endmill	[mm]
$\mathbf{r}$	General coordinate, deflection vector	[mm]
$\mathbf{s}$	Cutting edge position vector	[mm]
t	Time increment	[sec]
u, v	Nodal displacements, x and y-component of the tool deflection, respectively	[mm]
v_c	Cutting speed	[m/min]
$\mathbf{w}$	Workpiece description vector	[mm]
$\mathbf{w_0}$	Blank part description vector	[mm]
ε	Helix angle	[rad]
δ	Chip space ratio	[1]
φ	Rotation angle of the tool	[rad]
θ	Polar coordinate of the cross-section	[rad]
$\theta_{j,x}, \theta_{j,y}$	Nodal coordinates, rotation around x and y axis, respectively	[rad]
ϕ	Tooth pitch angle	[rad]
ψ	Cutting edge position angle	[rad]
ω_n	Natural frequency of the system	[Hz]
Ω	Angular velocity of the spindle	[rad/s]
ξ_l	Damping ratio of the l^{th} natural frequency of the spindle	[1]

1. Introduction

The performance of a milling process is mainly limited by vibrations generated by the process. The milling process generates dynamic cutting forces within a large frequency range. Depending on the dynamic behavior of the machine tool, heavy vibrations can occur. There are two essential types of vibrations [1].

The first and most harmful type of vibration is the so-called “chatter” which is a kind of a self-excited vibration caused by the regenerative effect of the machined surface [1, 2, 3]. The chip thickness depends on the current position of the cutting edge and the past position of the previous cutting edge of the mill. Consequently, the mathematical description of this phenomenon leads to a time delayed differential equation. In order to predict this type of vibration, the so-called stability chart must be created as a function of the technological process parameters. This calculation can be carried out in several ways like using the semi-discretization method [4, 5, 6], temporal finite elements [7, 8], multifrequency analysis approach [9, 10, 11] or time domain simulation [11, 12]. As shown in [13], the dominant chatter frequencies differ from the tooth engagement frequency, which causes aperiodic vibrations. Such vibrations typically create strong chatter marks on the milled surface [12, 14, 15].

The second type of vibration is the forced vibration caused by the periodically changing cutting force. This forced vibration can also have large amplitudes at resonant spindle speeds [16, 17], but still, the surface roughness which is measured along the feed direction is usually relatively small because the period of the forced vibration is the same as the forcing tooth engagement frequency.

To separate the influences of the two kinds of vibrations, the static deflection of the tool also has to be taken into account. It is shown in [16] that in case of helical fluted endmill, the machined surface shows large shape deviations. Especially, the surface profile in the axial direction of the tool is strongly influenced by the changing cutting forces and deflections [18, 19].

The main goal of this work is to evaluate machining operations during the process, based on quality related indicators. Therefore, the degradation of surface quality due to process generated vibrations is evaluated using a dynamic endmill and spindle model on one side, and using a process model on the other side. In the present study, the dynamic behavior of the system is described by coupling two different methods. In the first one, the spindle of the machine tool is analyzed based on the frequency response measurements [20, 21]. The second part determines the dynamic behavior of a general tool using Timoshenko beam elements with axial, torsional, and lateral dynamics [22, 23].

The measured resultant cutting force is applied to the governing equation of the coupled systems. In this case, there is no need to create advanced force calculation for the

precise description, which contains all the known and unknown phenomena (like non-linear force characteristic, short regenerative effect, process damping, state dependent delay, runout). The accuracy of the presented method depends only on the accuracy of the measured force signals and the coupled dynamic model of tool and machine tool. The calculated motions based on the measured forces describe the periodic forced vibrations, the chatter vibrations, and even the transient vibrations.

2. Development of a dynamic tool model

In order to simulate the dynamic motion of the tool during a material removal process, a tool model was developed which is applicable for endmill geometries and peripheral milling operations. In the dynamic model of the process, the workpiece is assumed to be perfectly rigid. Only the dynamic behavior of the tool and machine tool side is considered. To analyze the forced motion of the coupled tool and machine tool structure, described by the general coordinate $\mathbf{r}$, the governing equation of the obtained system can be determined in the following form:

$$\mathbf{M}\ddot{\mathbf{r}}(t) + \mathbf{C}\dot{\mathbf{r}}(t) + \mathbf{K}\mathbf{r}(t) = \mathbf{F}(t), \qquad (1)$$

where $\mathbf{M}$, $\mathbf{C}$ and $\mathbf{K}$ are global mass, damping and stiffness matrices, respectively, and $\mathbf{F}(t)$ is the resultant force. The dynamic model consists of two coupled parts. The first part describes the dynamic behavior of the spindle, based on the measured frequency response function (FRF). In the second part, the dynamic properties of the tool are calculated using a finite element beam model. The two parts are coupled by concatenating the mass, the damping and the stiffness matrices of the two parts.

2.1. Dynamic model of the spindle part

The FRF of the spindle is specific for a machine tool and has to be measured only once. The modal parameters (natural frequency $\omega_{n,l}$, damping ratio ξ_l and the modal constant B_l) for the l^{th} mode are determined by fitting rational fraction polynomials, which is a widely used procedure in the industry [20, 21]. The dynamic properties of the spindle can be characterized in its modal space given by the diagonal matrices.

$$\mathbf{M}^{\mathrm{S}}_{FRF} = \left[\frac{1}{B_l}\right], \quad \mathbf{C}^{\mathrm{S}}_{FRF} = \left[\frac{2\xi_l\omega_{n,l}}{B_l}\right], \quad \mathbf{K}^{\mathrm{S}}_{FRF} = \left[\frac{\omega^2_{n,l}}{B_l}\right]. \qquad (2)$$

The coupling of the two systems is defined along the Cartesian coordinates of the contact points between tool and machine tool. These are given by means of the sum of the modal coordinates q_l^s, therefore the general coordinates of the spindle part $r^{\mathrm{s}}(t)$ are redefined as follows:

$$\begin{aligned} \mathrm{r}_l^s(t) &= \mathrm{q}_l^s(t) \quad l = 1,2,\dots,N_m - 1, \\ \mathbf{r}_{N_m}^s(t) &= \textstyle\sum_{l=1}^{N_m} \mathbf{q}_l^s(t), \end{aligned} \tag{3}$$

where N_m is the number of the modeled eigenmodes of the spindle. The inverse transformation of Eq (3) is given by the transformation matrix $\widetilde{\mathbf{T}}$ as follows:

$$\mathbf{q}^{\mathrm{s}}(t) = \begin{bmatrix} q_1^s(t) \\ q_2^s(t) \\ \vdots \\ q_{N_m}^s(t) \end{bmatrix} = \widetilde{\mathbf{T}}\mathbf{r}^{\mathrm{s}}(t) = \begin{bmatrix} 1 & 0 & \cdots & 0 \\ 0 & 1 & \cdots & 0 \\ \vdots & \vdots & \ddots & \vdots \\ -1 & -1 & \cdots & 1 \end{bmatrix} \begin{bmatrix} r_1^s(t) \\ r_2^s(t) \\ \vdots \\ r_{N_m}^s(t) \end{bmatrix}. \tag{4}$$

The mass, damping and stiffness matrices are transformed into the space of these new coordinates with the same transformation matrices $\widetilde{\mathbf{T}}$:

$$\mathbf{M}_{gen}^{\mathrm{s}} = \widetilde{\mathbf{T}}^{\mathrm{T}}\mathbf{M}_{FRF}^{\mathrm{s}}\widetilde{\mathbf{T}},\ \mathbf{C}_{gen}^{\mathrm{s}} = \widetilde{\mathbf{T}}^{\mathrm{T}}\mathbf{C}_{FRF}^{\mathrm{s}}\widetilde{\mathbf{T}},\ \mathbf{K}_{gen}^{\mathrm{s}} = \widetilde{\mathbf{T}}^{\mathrm{T}}\mathbf{K}_{FRF}^{\mathrm{s}}\widetilde{\mathbf{T}}. \tag{5}$$

This method is used both in $\boldsymbol{x}$ and $\boldsymbol{y}$ direction separately. If we assume that there is no cross coupling between the two directions, the governing equation of the spindle system can be described by block diagonal matrices created from the direct sum of the matrices (Eq. (5)) in $\boldsymbol{x}$ and $\boldsymbol{y}$ direction.

$$\begin{bmatrix} \mathbf{M}_{gen}^{\mathrm{s},x} & \mathbf{0} \\ \mathbf{0} & \mathbf{M}_{gen}^{\mathrm{s},y} \end{bmatrix} \begin{bmatrix} \ddot{\mathbf{r}}^{\mathrm{s},x}(t) \\ \ddot{\mathbf{r}}^{\mathrm{s},y}(t) \end{bmatrix} + \begin{bmatrix} \mathbf{C}_{gen}^{\mathrm{s},x} & \mathbf{0} \\ \mathbf{0} & \mathbf{C}_{gen}^{\mathrm{s},y} \end{bmatrix} \begin{bmatrix} \dot{\mathbf{r}}^{\mathrm{s},x}(t) \\ \dot{\mathbf{r}}^{\mathrm{s},y}(t) \end{bmatrix} + \begin{bmatrix} \mathbf{K}_{gen}^{\mathrm{s},x} & \mathbf{0} \\ \mathbf{0} & \mathbf{K}_{gen}^{\mathrm{s},y} \end{bmatrix} \begin{bmatrix} \mathbf{r}^{\mathrm{s},x}(t) \\ \mathbf{r}^{\mathrm{s},y}(t) \end{bmatrix} = \mathbf{0}. \tag{6}$$

Note, that the general force is zero due to the spindle having no external excitation. We assume that the shaft is torsional rigid.

2.2. Dynamic model of the tool part

The mass, damping and stiffness matrices of the tool could be generated in the same way as the matrices of the spindle. However, if the mode shapes of the tool have to be

modeled [21, 24], then the measurements have to be made in multiple points along the tool length and more advanced methods are needed for the evaluation of the system matrices. Furthermore, several different endmills are used in the industry and measurement of each tool step-by-step would take unacceptably long time.

Consequently, the dynamic behavior of the tool is calculated by a finite element method (FEM). This method can sufficiently predict the dynamic properties of the tool (like stiffness and natural frequency) due to the fact, that the endmill tool is usually a monolithic part, and does not contain any joints or contact surfaces that could cause inaccuracies. Note, that the mode shapes of the tool are also included in this method. For the finite element model of the tool a parametrical description of the endmill geometry was developed. The aim of the developed endmill model is to get a detailed description of the endmill geometry, using a minimum of describing parameters. Therefore, the tool geometry is described by commonly used parameters [25], like the tool radius *R*, number of edges *N*, helix angle ε and the length of cutting edges z. In order to calculate the variation of stiffness along the tool axis, the cross-section zone was modeled for several slices of the endmill. The boundary curve $\mathbf{b}$ of the cross-section of the endmill at height z can be described by the simplified equation:

$$\mathbf{b}(z) = \begin{bmatrix} R(1-\delta\cdot\cos(\phi))\sin(\theta-\psi(z)) \\ R(1-\delta\cdot\cos(\phi))\cos(\theta-\psi(z)) \end{bmatrix}, \quad \begin{matrix} \theta \in [0,2\pi] \\ \phi = N/4\ \cdot \mathrm{mod}(\theta, 2\pi/N) \end{matrix}; \quad \psi(z) = \frac{z}{R}\tan(\varepsilon), \tag{7}$$

where θ is the polar coordinate of the tool, ϕ is the tooth pitch angle and ψ is the cutting edge position angle. The tool cross-section is represented by the nominal radius of the tool *R*, the number of edges *N,* the chip space ratio δ and the helix angle ε. The related sampled boundary curve is a polygon defined by the x and y coordinates of the points that are collected in the matrix ($\hat{\mathbf{b}} \in \mathbb{R}^{2xN_{points}}$). The generated cross-section simplifies the complex shape of a real tool cross-section by a minimum of describing parameters (see Fig. 1):

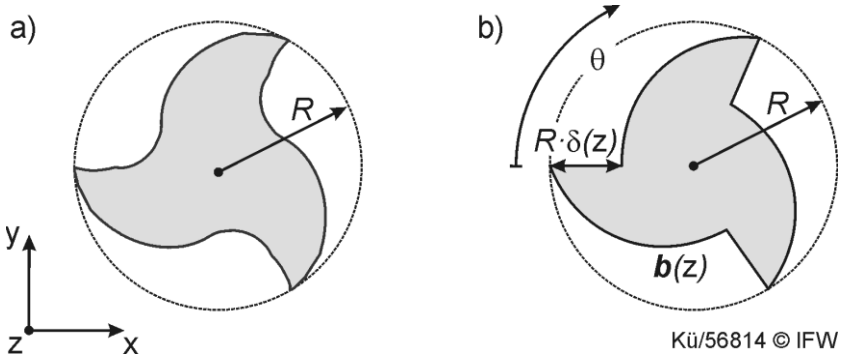

Fig. 1: Real cross-section of an endmill a) and simplified parametric cross-section b)

The variation of the cross-section geometry along the tool axis z is thereby describable by the variation of chip space ratio $\delta(z)$. In case of a helical tool, the cutting edge position angle $\psi(z)$ also depends on the axial position. This way, the parametric model is able to generate the cross-section geometry of the tool along the cutting edge length, the tool shaft and even for the tool chuck, where the radius also depends on the axial position $R(z)$.

In order to calculate the stiffness of the tool, the areas and moments of inertia of the cross-section are calculated using the trapezoidal method for polygonal sampled cross-sections:

$$A(z) = \frac{1}{2}\sum_{k=1}^{l}(y_{k+1}x_k - y_k x_{k+1}), \tag{8}$$

$$I_{xx}(z) = \frac{1}{12}\sum_{k=1}^{l}[y_{k+1}^2 + (y_k + y_{k+1})y_k]\,(y_{k+1}x_k - y_k x_{k+1}),$$
$$I_{yy}(z) = \frac{1}{12}\sum_{k=1}^{l}[x_{k+1}^2 + (x_k + x_{k+1})x_k]\,(x_{k+1}y_k - x_k y_{k+1}). \tag{9}$$

Note, that $I_{xx} = I_{yy}$ and $I_{xy} = I_{yx} = 0$ if the tool has at least 3 cutting edges.

The discretization of the tool along the z axis is represented in Fig. 2. The number of beam elements N_b depends on the desired number of the modeled eigenmodes of the tool and the required accuracy of the surface generation.

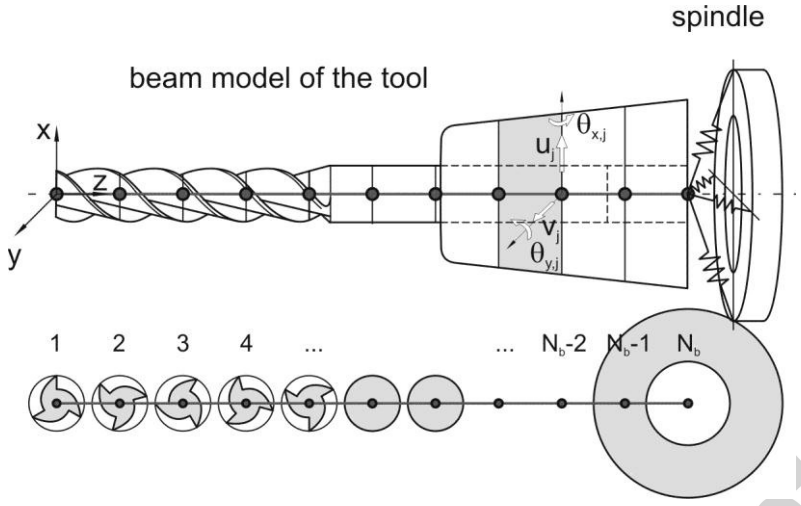

Fig. 2: Representation of the beam model with changing cross-sections and the connection to the spindle

According to the reconstruction of surface topography, the dominant bending modes of the endmill will mostly influence the machined surface topography. Hence, beam theory was chosen for the endmill modeling. Based on the Timoshenko's beam theory [26, 27, 28] the bending of the j^{th} node of the tool's beam element can be described by four degrees of freedom:

$$\mathbf{r}_j^b = \left[u_j, v_j, \theta_{j,x}, \theta_{j,y}\right], \qquad (10)$$

where u and v are the lateral movement in x and y direction, respectively, and θ_x and θ_y are the rotation around the x and y axis, respectively. The mass and stiffness matrices of one beam segment are determined based on [22] by using the area and the moments of inertia of the current cross-section (see Eq. (8) and Eq. (9)), and the material properties of the tool (density, Poisson ratio and Young's modulus). The global mass and stiffness matrices of the beam model of the tool are built up according to the neighboring elements [26]. The governing equation of the tool dynamic is given by:

$$\mathbf{M}_{glob}^{\mathrm{b}}\ddot{\mathbf{r}}^{\mathrm{b}}(t) + \mathbf{C}_{glob}^{\mathrm{b}}\dot{\mathbf{r}}^{\mathrm{b}}(t) + \mathbf{K}_{glob}^{\mathrm{b}}\mathbf{r}^{\mathrm{b}}(t) = \mathbf{F}(t), \qquad (11)$$

where the global damping matrix $\mathbf{C}_{glob}^{\mathrm{b}}$ is calculated from the stiffness matrix: $\mathbf{C}_{glob}^{\mathrm{b}} = \eta\mathbf{K}_{glob}^{\mathrm{b}}$.

In the computation, the frequency-independent damping coefficient η was chosen to create the typical damping ratio $\xi_1 = 1\%$ on the first mode. Its value can be calculated by:

$$\eta = \frac{2\xi_1}{\omega_{n,1}}, \qquad (12)$$

where the first natural frequency of the tool $\omega_{n,1}$ is computed from the well-known characteristic polynomial:

$$\det\left(-\omega_{\mathrm{n}}^2 \mathbf{M}_{glob}^{\mathrm{b}} + \mathbf{K}_{glob}^{\mathrm{b}}\right) = 0. \qquad (13)$$

2.3. Global system matrices

As shown in Fig. 2, a flexible connection is modeled between the spindle and the tool. In section 2.1, only the general coordinates of the spindle in x and y directions are defined. Thus, coupling of the matrices can be done between the variables $r_{N_{m,x}}^{s,x}$ and u_{N_b}, and $r_{N_{m,y}}^{s,y}$ and v_{N_b} by considering linear spring (k_x^{ce}, k_y^{ce}) and damping (c_x^{ce}, c_y^{ce}) elements between the coordinates. The stiffness and damping matrices of the coupling element for the $\left[\mathrm{r}_{N_{m,x}}^{s,x} \;\; u_{N_b}\right]^T$ coordinates are given by:

$$\mathbf{K}_{elem}^{coup} = \begin{bmatrix} k_x^{ce} & -k_x^{ce} \\ -k_x^{ce} & k_x^{ce} \end{bmatrix}, \quad \mathbf{C}_{elem}^{coup} = \begin{bmatrix} c_x^{ce} & -c_x^{ce} \\ -c_x^{ce} & c_x^{ce} \end{bmatrix}. \qquad (14)$$

The coupling matrices along the y direction have a similar form. Due to the infinite torsional stiffness of the spindle, the torsional coupling can be modeled by torsional spring $k_{\theta x}^{ce}$ and torsional damping $c_{\theta x}^{ce}$ elements between the variable $\theta_{N_b,x}$ and the ground (same applies for $\theta_{N_b,y}$). The final governing equation has the same form as Eq. (1) with general coordinates $\mathbf{r} = \left[\, \mathbf{r}_1^b \;\; \mathbf{r}_2^b \;\; \ldots \;\; \mathbf{r}_{N_b}^b \;\; \mathbf{r}^{s,x} \;\; \mathbf{r}^{s,y} \,\right]^T$. Fig. 3 represents the pattern of the coupled stiffness matrix. In the computation, the local moments on the beam elements are neglected, and only the cutting forces in x and y direction are applied on the coordinates u_j and v_j $(j = 1,2 \ldots N_{act})$. These coordinates belong to the active cutting length, where the z_j coordinate of the j^{th} cross-section is smaller than the depth of cut a_p.

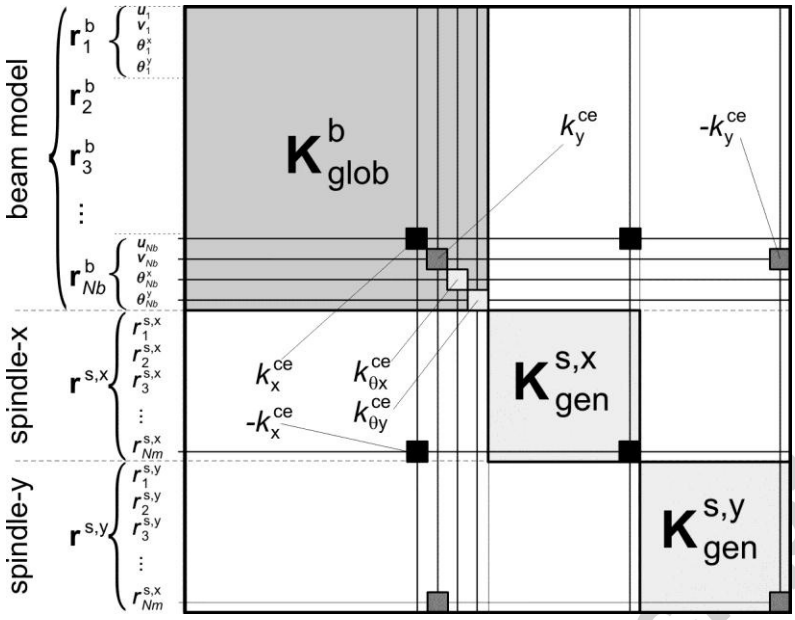

Fig. 3: Pattern of the coupled symmetric stiffness matrix (white regions denote the zero elements)

2.4. Forced motion

The main goal of the developed method is to apply measured cutting forces on the endmill model and to estimate the surface quality based on the forced motion. During the cutting process the resultant forces in the x, y and z direction are provided by a force dynamometer. It is obvious, that forces acting on the cutting edges are complex distributed, but for the forced motion it is supposed that the measured cutting force is distributed uniformly along the active engagement zone. This assumption is illustrated in Fig. 4.

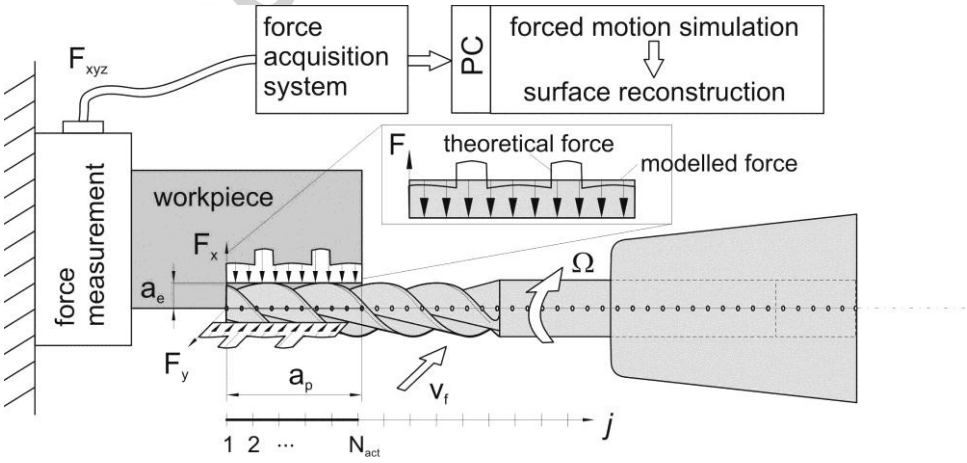

Fig. 4: The measurement setup and the modeled uniform force distribution

The generation of the forced motion based on full matrices in Eq. (1) would take too much computational effort due to the large matrices. Therefore, the system is reduced

by means of the modal transformation [21, 24]. The system is transformed into the modal space from the space of the general coordinates ($\mathbf{Tq} = \mathbf{r}$) as follows:

$$\mathbf{T}^{\mathrm{T}}\mathbf{M}\mathbf{T}\ddot{\mathbf{q}}(t) + \mathbf{T}^{\mathrm{T}}\mathbf{C}\mathbf{T}\dot{\mathbf{q}}(t) + \mathbf{T}^{\mathrm{T}}\mathbf{K}\mathbf{T}\mathbf{q}(t) = \mathbf{T}^{\mathrm{T}}\mathbf{F}(t), \qquad (15)$$

where the transformation matrix $\mathbf{T}$ contains the mode shapes $\mathbf{T} = \left[\mathbf{A}_1, \mathbf{A}_2, \dots \mathbf{A}_{N_b+N_{FRFx}+N_{FRFy}}\right]$ calculated by means of the eigenvalue problem:

$$\left(-\omega_{\mathrm{n,i}}^2\mathbf{M} + \mathbf{K}\right)\mathbf{A}_i = 0. \qquad (16)$$

The size of the system can be reduced by selecting only the important modes. In our case, only the first $N_{mod} = 50$ modes were modeled, and the truncated transformation matrix $\mathbf{T} = \left[\mathbf{A}_1, \mathbf{A}_2, \dots \mathbf{A}_{N_{mod}}\right]$ is used.

Equation (15) could be solved in the time domain, however, if periodic cutting processes are focused, the frequency domain solution is more appropriate. The forced motions of the selected modes are given by:

$$\mathbf{q}(\omega) = (-\omega^2\mathbf{T}^{\mathrm{T}}\mathbf{M}\mathbf{T} + i\omega\mathbf{T}^{\mathrm{T}}\mathbf{C}\mathbf{T} + \mathbf{T}^{\mathrm{T}}\mathbf{K}\mathbf{T})^{-1}\left(\mathbf{T}^{\mathrm{T}}\mathbf{F}(\omega)\right). \qquad (17)$$

During the computation the Fast Fourier Transformation (FFT) was used to transform the measured cutting force into the frequency domain and the Inverse Fast Fourier Transformation (IFFT) was used to determine the forced motion $\mathbf{q}(t)$ in time domain. For the surface generation, only the general coordinates of the active segments ($j = 1,2 \dots, N_{act}$, see Fig. 4) of the tool are required.

In this section a mechanical model is described, which can provide the motions of the tool in case of a given forcing. The time function of the forcing can be simulated or measured during the cutting process.

3. Generation of surface topography in peripheral milling

To be able to reconstruct the surface topography of peripheral milling processes, a detailed material removal model was developed. The model describes the tool and workpiece geometry as well as the relative movement of both. Some well-known parameters, like diameter of the tool D, number of teeth N, helix angle ε and process conditions (depth of cut a_p, width of cut a_e, feed per tooth f_z) are used. Thereby, the tool path $\mathbf{p}(t)$ can be described by:

$$\mathbf{p}(t) = \frac{\Omega t}{2\pi}\mathbf{f}_z N, \qquad (18)$$

where Ω is the angular velocity of the spindle and vector $\mathbf{f}_z$ describes the linear feed per tooth motion. Along this motion, the cutting edges are rotating around the Tool Center Point (TCP) by the rotation angle $\varphi(t) = \Omega t$. The cutting edge paths s_{ij} of the i^{th} cutting edge can be described on level j as a harmonic function:

$$\mathbf{s}_{ij}(t) = \begin{bmatrix} -R_{ij} \cdot \cos\left(\varphi(t) - \phi_{\mathrm{ij}} - \psi_j\right) \\ R_{ij} \cdot \sin\left(\varphi(t) - \phi_{\mathrm{ij}} - \psi_j\right) \end{bmatrix} + \mathbf{p}(t), \qquad (19)$$

$$\phi_{ij} = \frac{2\pi}{N}(i-1)\,; \qquad \psi_j = \frac{z_j}{R}\tan(\varepsilon),$$

where ϕ_{ij} is the cutting edge angle, which describes the current position of the i^{th} cutting edge and ψ_j is the cutting edge position angle at the j^{th} level. These equations describe the relevant motion of the cutting edges along the tool path in the $x-y$ plane. In the same way as the endmill has been described along the tool axis, the workpiece can be described as a number of polygons over the height of the workpiece z_W.

These polygons give the geometry of the blank part $\boldsymbol{w}_{j\,0}$ in the j^{th} level. It is now possible to describe the workpiece contour at one time step t as the subtraction of tool paths $\mathbf{s}_i$ - $\mathbf{s}_{i-1}$ and the previous workpiece contour $\boldsymbol{w}_{j\,t-1}$:

$$\mathbf{w}_{j\,t} = \mathbf{w}_{j\,t-1} \cap \overline{\left(\mathbf{s}_{ij} \cap \overline{\mathbf{s}_{i-1\,j}}\right)}. \qquad (20)$$

This can be done by Boolean operations like intersection and subtraction between the sampled polygons. The resulting geometry $\mathbf{w}_j$ in the j^{th} level contains the contour of the resulting workpiece (see Fig. 5).

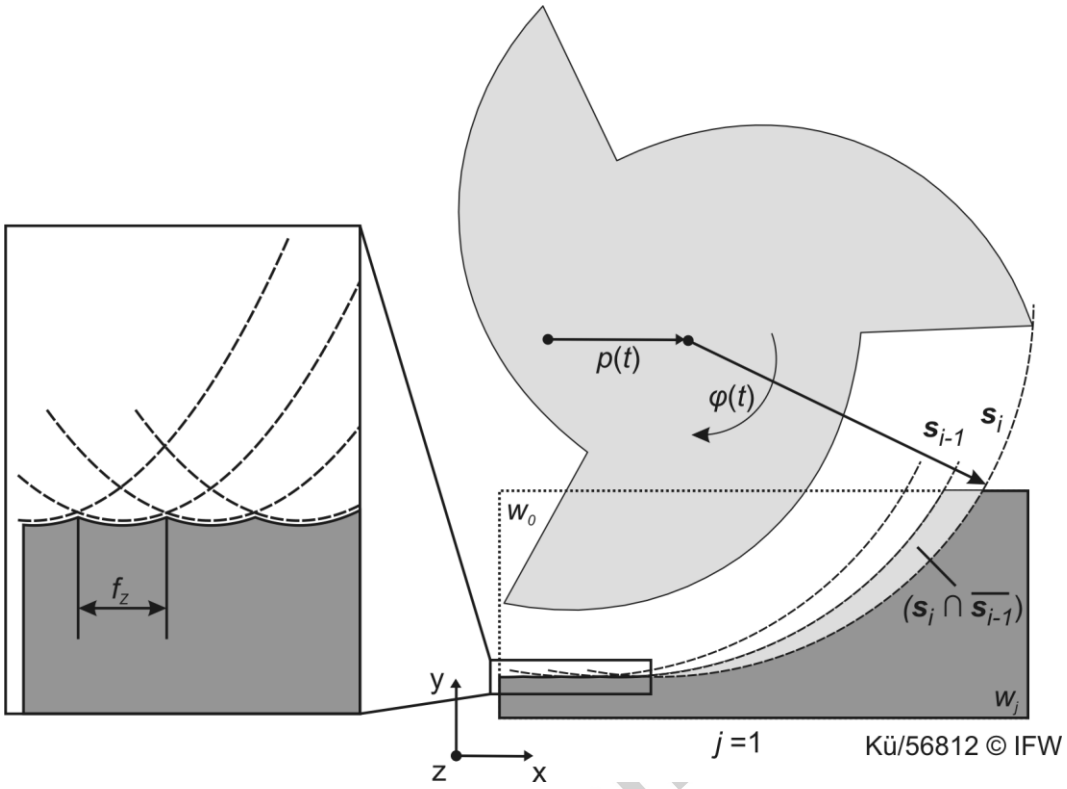

Fig. 5: Principle of the material removal calculation

By this method, the shape of the machined workpiece can be obtained, including the surface roughness of the machined contour. In real machining conditions, however, the contour of the machined surface is not only generated by the feed movement and the tool rotation, it is also influenced by vibrations and geometrical errors of the system which cause a relative movement between tool and workpiece. In order to implement these effects in the material removal process, the computed tool vibration $\mathbf{r}(t)$, described in section 2, is implemented. In the calculation of the machined surface, only the nodal motion of the tool is necessary , therefore, the deflection vector $[u_j, v_j]$ in the $x-y$ plane is required (see Eq. (10)). In order to calculate the workpiece contour caused by vibrations during the milling process in level *j*, deflections can be added to the cutting edge paths in Eq. (19):

$$\hat{\mathbf{s}}_{ij}(t) = \begin{bmatrix} -R_{ij} \cdot \cos\left(\varphi(t) - \phi_{\mathrm{ij}} - \psi_j\right) \\ R_{ij} \cdot \sin\left(\varphi(t) - \phi_{\mathrm{ij}} - \psi_j\right) \end{bmatrix} + \mathbf{p}(t) + \begin{bmatrix} u_j(t) \\ v_j(t) \end{bmatrix}. \qquad (21)$$

Using this additional term, it is possible to include the dynamic motion of the endmill during the cutting process.

In order to simulate the shape of the machined workpiece, a level curve representation of the workpiece is used [29]. The material removal procedure (Fig. 5) is done separately for each level curve of the workpiece. The generated level curves of the machined workpiece incorporate the geometrical profile of the machined surface.

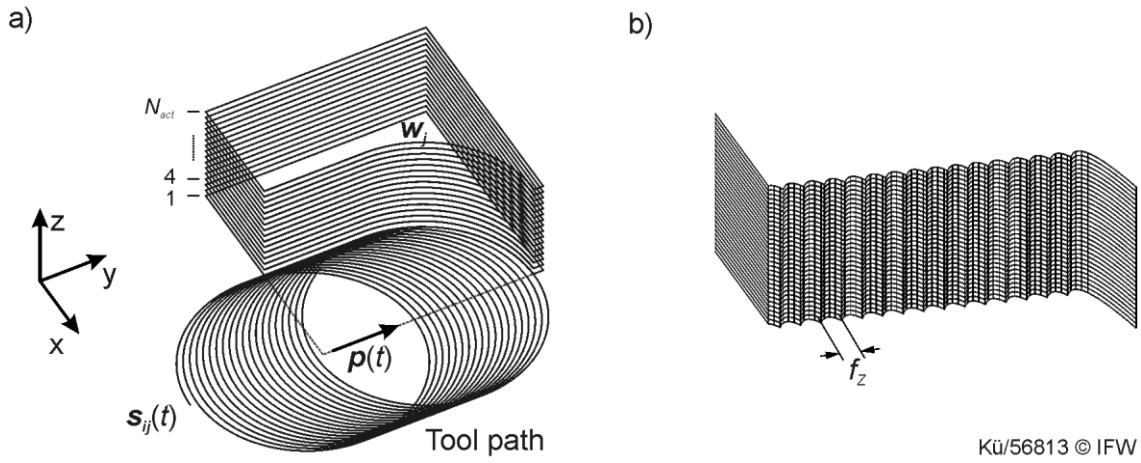

Fig. 6: Generation of the 3-dimensional workpiece model a) and meshed surface topography of the machined workpiece b)

Such profile contains surface roughness caused by the feed movement of the endmill (Fig. 5). If some additional movements of the tool are implemented, it also incorporates the surface shape due to occurring tool vibrations $\mathbf{r}(t)$. The workpiece model contains a 2½-dimensional representation of the workpiece volume. Thereby, it shows discrete information along the vertical direction z. Depending on the discretization of the tool and the workpiece geometry the vertical shape of the machined workpiece can be examined. To be able to examine the surface characteristics, the surface shape was meshed and interpolated to receive a smooth mesh of the machined surface. The meshed surface can be compared to the requested surface shape and thereby, quality indicators like surface roughness and shape deviation of the machined workpiece can be inspected, like it is shown in [16].

4. Experimental verification

In order to evaluate the developed method, the reconstruction of machined surfaces is carried out for measured cutting forces and the reconstructed surface topographies are compared to the measured workpiece surfaces.

4.1. Description of the experimental setup

To implement the dynamic behavior of the machine tool into the global system matrix (see section 2), the dynamic response of the machine tool spindle was analyzed while the structure was excited. This was done by a laser vibrometer using the impact hammer method. The response was captured in two orthogonal directions. Thereby, it was found,

that the frequency response function of the spindle system is almost symmetric, so the cross effects are neglected in this model.

In the finite element beam model of the tool, the geometric data and the material data of the endmill are used (see Table 1). During the computation, $N_b = 250$ nodes and the system coupling parameters of [22] in table 2 were used. The first important natural frequencies and mode shapes are plotted in Fig.7 by using a meshed level curve representation of the tool.

Table 1: Geometrical data and material properties of the milling tool

Diameter	10 mm	Cutting length	50 mm	Young's modulus	220 GPa
Number of edges	3	Total length	115 mm	Poisson number	0.33
Helix angle	45 °	Chip space ratio	50 %	Density	7.8 kg/dm^3

Table 2: System coupling parameters [22]

	Latheral		Bending (x,y)	
Stiffness	k_x^{ce}, k_y^{ce}	$300\ \frac{N}{\mu m}$	$k_{\theta x}^{ce}, k_{\theta y}^{ce}$	$1.6 \cdot 10^6\ \frac{Nm}{rad}$
Damping	c_x^{ce}, c_y^{ce}	$182\ \frac{Ns}{m}$	$c_{\theta x}^{ce}, c_{\theta y}^{ce}$	$1240\ \frac{Nms}{rad}$

ω_1=1467 Hz ω_2=1467 Hz ω_{10}=2335 Hz ω_{26}=6683 Hz ω_{47}=21490 Hz

Fig. 7: Representation of the magnified modes of the coupled tool-spindle system

For the examination of tool dynamics in milling processes, an experimental setup was designed. The setup is illustrated in Fig. 4. During a peripheral milling process, the cutting forces were measured by a three component force dynamometer (Kistler 9257 B). The experimental parameters were chosen for the variation of spindle speed and constant engagement conditions:

Table 3: Process parameters for the experimental milling processes

Nr.	1	2	3	4	5	6	7	8	9	10
a_p [mm]	16									
a_e [mm]	1									
f_z [mm]	0,05									
v_c [m/min]	40	60	80	100	120	140	160	180	200	220
f_{te} [Hz]	63,7	95,5	127,3	159,2	191,0	222,8	254,6	286,5	318,3	350,1
n [rpm]	1.273	1.910	2.546	3.183	3.820	4.456	5.093	5.730	6.366	7.003

By varying the cutting velocity v_c, the tooth engagement frequency f_{te} was changed in ten steps. Thereby, the excitation of the machine tool was influenced. Ten different milling processes were performed by measuring the cutting forces in the workpiece coordinates. Afterwards, the surface topographies of the machined surfaces were captured by a confocal laser microscope. The experimental results are compared to the reconstructed surface topographies in the next section.

4.2. Reconstruction of surface topographies

In the first experimental run, moderate process conditions were chosen to be able to validate the influence of tool deflection and surface generation mechanism. The first milling process was performed using the parameter set 1 (Table 3). The milling process was found to be stable, concerning that there are no resulting vibration near to any natural frequency of the tool and machine tool structure.

The cutting forces from the milling process were recorded and applied to the dynamic tool model, as described in section 2.4. The machined surface was reconstructed by applying the tool motion to the material removal model. The measured (a) and reconstructed surface topography (b) is compared in Fig. 8:

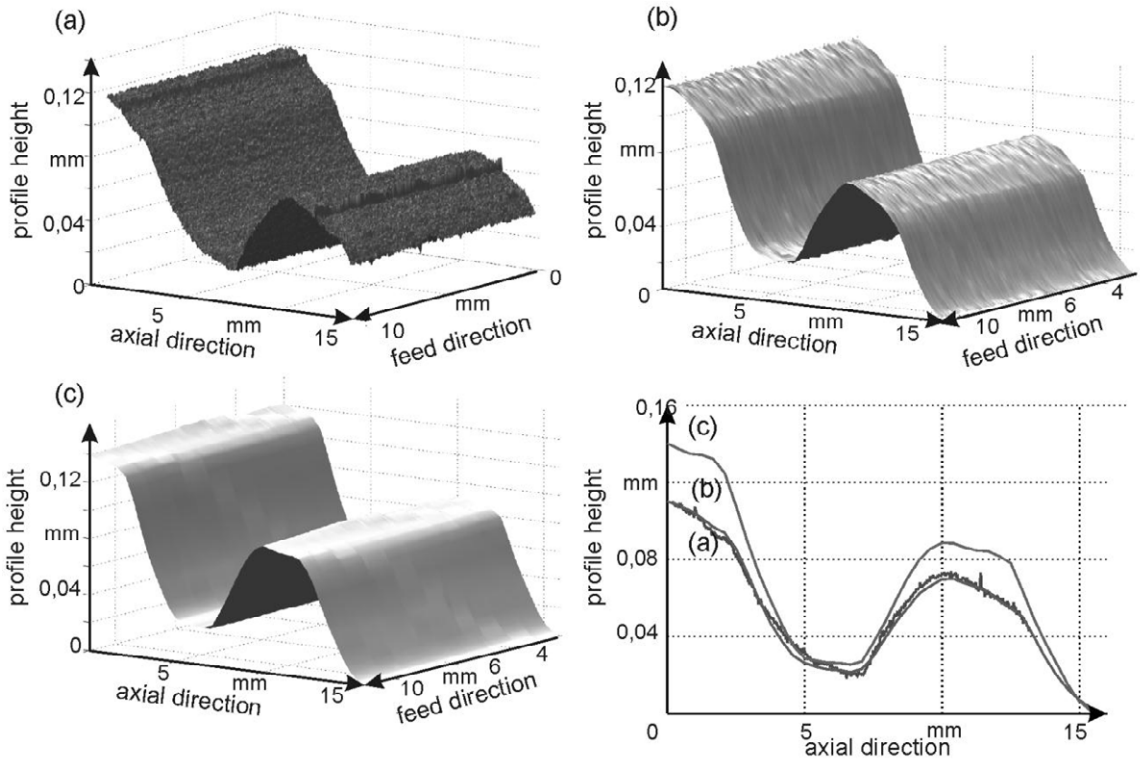

Fig. 8: Measured surface topography a) and reconstructed surface based on the measured cutting force b) and the theoretical cutting forces c) for parameter set 1

As it can be seen from the measured surface, the topography contains a characteristic shape in the axial direction. Surface roughness can also be obtained from the measured surface, but it is affected by measurement noise. The surface roughness of the reconstructed surface (Fig. 8 b) includes some additional noise from the measured cutting forces. The agreement of the characteristic shape of the machined surface can be obtained from the profiles of topography a) and b). Referring to this validation for moderate process conditions, the developed method for the reconstruction of surface topographies shows good agreement between measured and reconstructed surface shapes even in case of the first verification. In order to verify the developed model, a third test case was performed by using theoretically calculated cutting forces. The simulated cutting forces do not include any process vibration or measurement noise, thereby the influences on surface generation can be separated. The used cutting force model delivers accurate cutting forces for several peripheral milling processes [30]. Computed cutting forces were applied to the tool model and the resulting deflections were used for the simulation of the theoretical surface topography (Fig. 8 c). It can be seen, that surface roughness is very small due to uniform engagement conditions and the absence of measurement noise. The nominal profile shape of the measured surface topography could not be predicted well, because the cutting force model was implemented in an open loop. Thereby, the material removal and cutting force generation is not influenced by the tool deflection. In this case, the developed method

for the reconstruction of surface topographies from measured cutting forces delivers qualitative information for the validation of milling processes. Furthermore, the developed method is able to reconstruct transient changes in the cutting conditions. Figure 9 shows a comparison between measured and reconstructed topography for an emerging cut. It can be seen that the shape of the two surfaces fits well both in the axial and in the feed direction. The slope of the surface in the feed direction at the end of the process is also predicted properly.

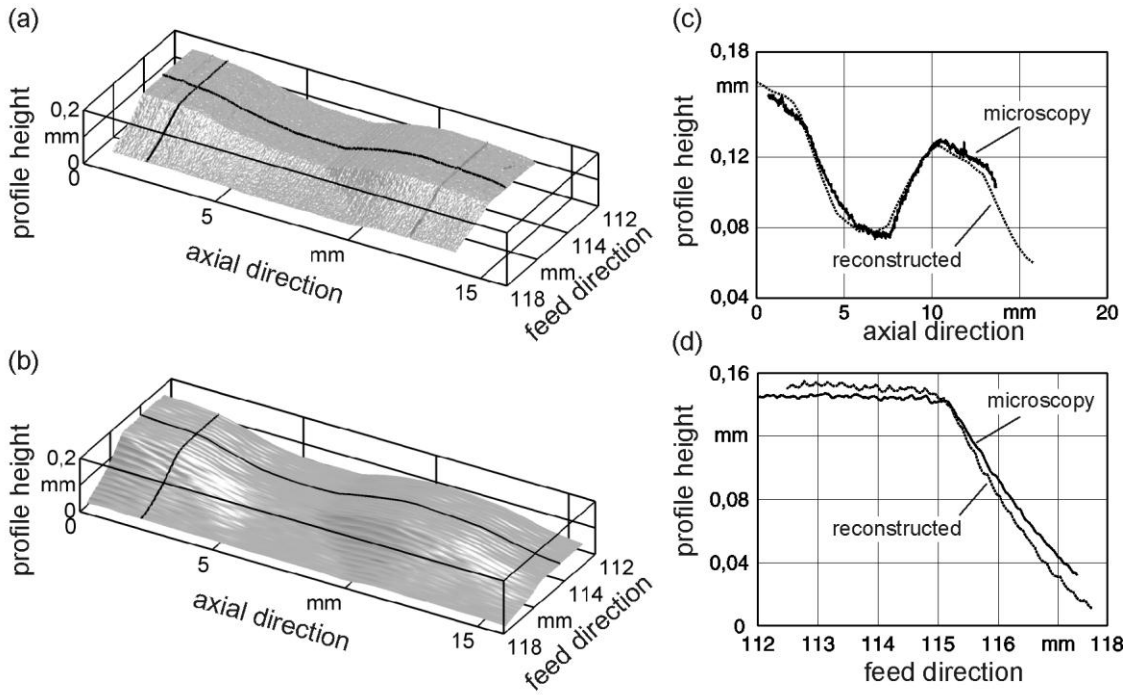

Fig. 9: Measured a) and reconstructed b) surface created by a transient vibration at the end of process 1. The surface profile along the tool axis c) and the surface profile along the feed direction d) are plotted along the black lines in a) and b)

Additionally, the reconstruction of surface topographies was verified for unstable process conditions. The measured cutting forces can easily be applied in the model in the presence of chatter. The measured and reconstructed surfaces for a milling process (Table 3 No. 8) with chatter vibration is shown in Fig. 10. Due to the necessary simplifications of the model of system dynamics, some deviations can be seen in the occurrence of dynamic surface marks. The reconstructed surface roughness is higher than the measured one but the characteristic of the chatter marks are similar.

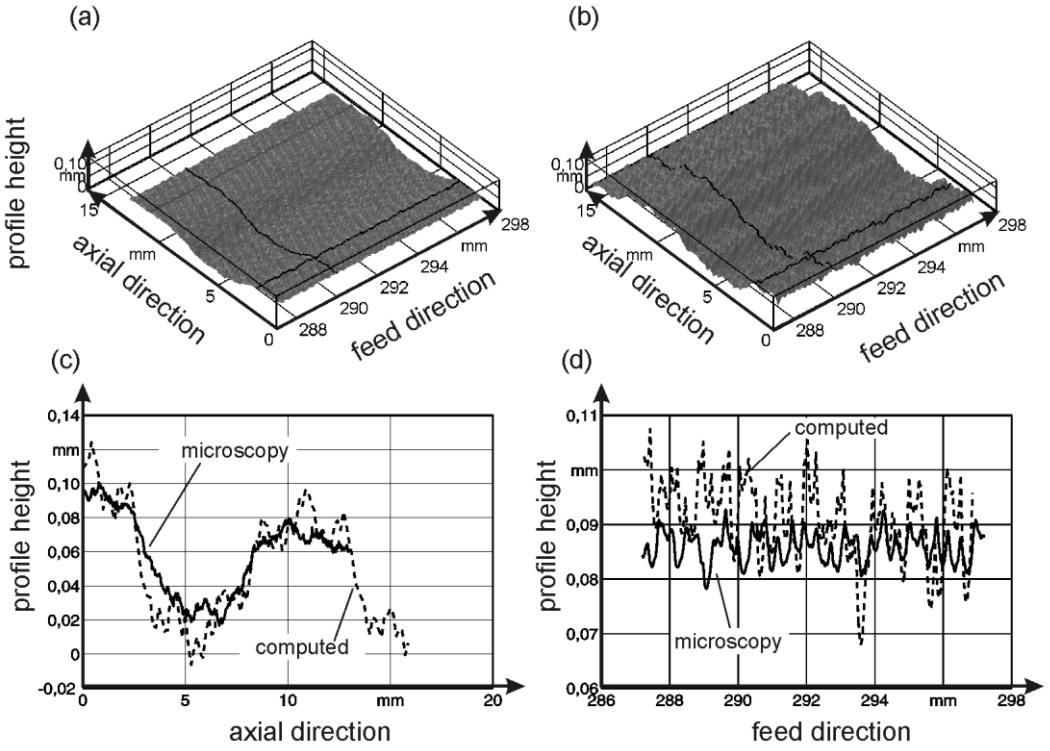

Fig. 10: The measured a) and the reconstructed b) surfaces created by a slight chatter vibration during process 8. The surface profile along the tool axis c) and the surface profile along the feed direction d) are plotted along the black lines in a) and b)

In case of chatter vibration, the presented method provides rather qualitative predictions for the machined surface. Depending on the application of the developed method, however, the reconstruction of workpiece quality for unstable process conditions will not be relevant, as long as process monitoring strategies will identify instability. Especially, for the task of process monitoring, the developed method will aim the understanding of process signals and will provide online evaluation criterion for quality related information from manufacturing processes.

5. Conclusion and Outlook

This paper presents a method for the reconstruction of surface topographies of machined surfaces based on the measured resultant cutting forces. By representing the dynamic behavior of the machine tool and milling tool within a receptance coupling dynamic model, the tool motion during the milling process can be reconstructed. This, together with the measured cutting forces captured by a force dynamometer, and with the parameters of the engagement conditions of the peripheral milling process, the machined workpiece topography can be estimated accurately under moderate cutting conditions.

The comparison of the measured and the reconstructed surface topographies verified during experimental test runs also presented the limitations of the method. For stable cutting conditions, the developed method delivers an accurate reconstruction of the surface shape, and even for transient process conditions, the reconstruction delivers adequate results, too, since these are all the consequences of external dynamic excitations. The implemented method was also applied in case of chatter (self-excited) vibrations. In this case, however, the developed method is able to predict the characteristic shape of the machined surface qualitatively only, while the information on the roughness provides sufficient indication of the appearance of chatter.

Although, the proposed methodology does not provide qualitatively reliable monitoring of the machined surface for extreme cutting conditions like in the case of chatter, it can work perfectly under moderate cutting conditions like in the case of finishing operations. This is true under the conditions that the model parameters, e.g. stiffness and damping, are obtained in several open loop dynamic measurements of the machine tool components, and the cutting and engagement geometry is identified accurately.

Further development of the current configuration of the process model depends on concurrent design goals, which mainly are the accuracy, the performance and the flexibility of the approach. For further applications, the method has to be adapted either for higher accuracy, resulting in more complex models and increasing flexibility, or it has to be simplified in order to increase the performance for the online evaluation of process conditions in machining operations. The developed method has a great potential in online monitoring of the surface topographies during peripheral milling processes and this way, it may become an essential part of adaptive control strategies.

6. Acknowledgement

The results presented in this paper were obtained within the Collaborative Research Center 653 ‘‘Gentelligent Components in their Lifecycle’’ (TP-K2). The authors would like to thank the German Research Foundation for its financial and organizational support. The article are result of the activities performed within DYNXPERTS project, funded by the European Commission – FP7 Factories of the Future with the Grant Number 260073 and it is connected to the scientific program of the "Development of quality-oriented and harmonized R+D+I strategy and functional model at BME" project. This project is supported by the New Hungary Development Plan (Project ID: TÁMOP-4.2.1/B-09/1/KMR-2010-0002).

References

[1] S. A. Tobias, Machine Tool Vibration, Blackie and Son, Ltd., London, 1965.
[2] J. Tlusty, L. Spacek, Self-excited vibrations on machine tools, Prague, Nakl CSAV, (In Czech.), 1954.
[3] G. Stépán, Retarded Dynamical Systems, Longman, Harlow, 1989.
[4] T. Insperger, G. Stépán, Semi-discretization method for delayed systems, International Journal for Numerical Methods in Engineering 55 (2002) pp. 503–518.
[5] T. Insperger, G. Stépán, Semi-Discretization for Time-Delay Systems, 1st Edition, Applied Mathematical Sciences, Springer, 1, 2011.
[6] C. Henninger, P. Eberhard, Improving the computational efficiency and accuracy of the semi-discretization method for periodic delay-differential equations, European Journal of Mechanics A/Solids 27 (6) (2008) pp. 975–985.
[7] P. V. Bayly, J. E. Halley, B. P. Mann, Stability of interrupted cutting by temporal finite element analysis, Journal of Manufacturing Science and Engineering 125 (2) (2003) pp. 220–226.
[8] T. Insperger, B. P. Mann, G. Stépán, P. V. Bayly, Stability of up-milling and down-milling, part 1: alternative analytical methods, International Journal of Machine Tools and Manufacture 43 (1) (2003) pp. 25–34.
[9] S. D. Merdol, Y. Altintas, Multi frequency solution of chatter stability for low immersion milling, Journal of manufacturing science and engineering 126 (3) (2004) pp. 459–466.
[10] Y. Altintas, G. Stépán, D. Merdol, Z. Dombóvári, Chatter stability of milling in frequency and discrete time domain, CIRP Journal of Manufacturing Science and Technology 1 (1) (2008) pp. 35–44.
[11] M. Zatarain, J. Muñoa, G. Peigné, T. Insperger, Analysis of the influence of mill helix angle on chatter stability, CIRP Annals - Manufacturing Technology 55 (1) (2006) pp. 365–368.
[12] T. Surmann, D. Enk, Simulation of milling tool vibration trajectories along changing engagement conditions, International Journal of Machine Tools and Manufacture 47 (9) (2007) pp. 1442–1448, selected papers from the 2nd International Conference on High Performance Cutting.
[13] Z. Dombóvári, A. Iglesias, M. Zatarain, T. Insperger, Prediction of multiple dominant chatter frequencies in milling processes, International Journal of Machine Tools and Manufacture 51 (6) (2011) pp. 457–464.
[14] K. Weinert, T. Surmann, H. Müller, Modeling of surface structures resulting from vibrating milling tools, Production Engineering – Research and Development 13 (2) (2006) pp. 133–138.
[15] K. Weinert, T. Surmann, D. Enk, O. Webber, The effect of runout on the milling tool vibration and surface quality, Production Engineering – Research and Development 1 (3) (2007) pp. 265–270.
[16] D. Bachrathy, T. Insperger, G. Stépán, Surface properties of the machined workpiece for helical mills, Machining Science and Technology 13 (2) (2009) pp. 227–245.
[17] H. Paris, G. Peigne, R. Mayer, Surface shape prediction in high speed milling, International Journal of Machine Tools and Manufacture 44 (15) (2004) pp. 1567–1576.

[18] W. A. Kline, R. E. DeVor, J. R. Lindberg, The prediction of cutting forces in end milling with application to cornering cuts, International Journal of Machine Tool Design and Research 22 (1) (1982) pp. 7–22.
[19] P. Dépincé, J.-Y. Hascoët, Active integration of tool deflection effects in end milling. part 1. prediction of milled surfaces, International Journal of Machine Tools and Manufacture 46 (9) (2006) pp. 937–944.
[20] M. H. Richardson, D. L. Formenti, Parameter estimation from frequency response measurements using rational fraction polynomials, 1st IMAC Conference, Orlando, FL, 1982, p. 15.
[21] Z. Dombóvári, G. Stépán, Marószerszámok dinamikai tulajdonságai és azok hatása a megmunkálás stabilitására, GÉP accepted (2011) pp. 1–12, (in Hungarian).
[22] T. L. Schmitz, G. S. Duncan, Three-component receptance coupling substructure analysis for tool point dynamics prediction, Journal of Manufacturing Science and Engineering 127 (4) (2005) pp. 781–790.
[23] C. E. Okwudire, Y. Altintas, Hybrid modeling of ball screw drives with coupled axial, torsional, and lateral dynamics, Journal of Mechanical Design 131 (7) (2009) pp. 1–9.
[24] D. J. Ewins, Modal Testing: theory, practice and application, Research Studies Press, John Wiley & Sons Inc., England, 2000.
[25] S. Engin, Y. Altintas, Mechanics and dynamics of general milling cutters.: Part i: helical end mills, International Journal of Machine Tools and Manufacture 41 (15) (2001) pp. 2195–2212.
[26] D. H. Y. William Weaver, Stephen Timoshenko, Vibration problems in engineering, 5th Edition, John Wiley & Sons Inc., 1990.
[27] R. Davis, R. Henshell, G. Warburton, A timoshenko beam element, Journal of Sound and Vibration 22 (4) (1972) pp. 475–487.
[28] T. Yokoyama, Vibrations of a hanging timoshenko beam under gravity, Journal of Sound and Vibration 141 (2) (1990) pp. 245–258.
[29] C. Schmidt, Level curve based geometry representation for cutting force prediction, in: DAAAM International Symposium, Wien, 2006.
[30] B. Denkena, C. Schmidt, A flexible force model for predicting cutting forces in end milling, Production Engineering – Research and Development XIII/2 (2006) pp. 15–20.

Model Based Reconstruction of Milled Surface Topography from Measured Cutting Forces

Authors: Denkena, B.*; Krüger, M.*; Bachrathy, D.**; Stepan, G.***

1. Highlights:

The surface topographies of machined surfaces were reconstructed from measured cutting forces.

The behavior of spindle, machine tool and the endmill was modeled.

The machined surface was reconstructed based on a process model for milling operations.

Measured and reconstructed surfaces show good agreement for a range of milling processes.

The implemented method can also be applied in case of chatter vibrations.